01 Jun 2019

Impact of Anharmonicity on the Vibrational Entropy and Specific Heat of UO_2

M. S. Bryan

J. W. L. Pang

B. C. Larson

Aleksandr V. Chernatynskiy
Missouri University of Science and Technology, aleksandrc@mst.edu

et. al. For a complete list of authors, see https://scholarsmine.mst.edu/phys_facwork/1996

Recommended Citation

M. S. Bryan et al., "Impact of Anharmonicity on the Vibrational Entropy and Specific Heat of UO_2," *Physical Review Materials*, vol. 3, no. 6, American Physical Society (APS), Jun 2019.
The definitive version is available at https://doi.org/10.1103/PhysRevMaterials.3.065405

Impact of anharmonicity on the vibrational entropy and specific heat of UO_2

M. S. Bryan,[1,*] J. W. L. Pang,[1] B. C. Larson,[1] A. Chernatynskiy,[2] D. L. Abernathy,[3] K. Gofryk,[4] and M. E. Manley[1,†]

[1]*Materials Science and Technology Division, Oak Ridge National Laboratory, Oak Ridge, Tennessee 37831, USA*

[2]*Department of Physics, Missouri University of Science and Technology, Rolla, Missouri 65409, USA*

[3]*Neutron Scattering Division, Oak Ridge National Laboratory, Oak Ridge, Tennessee 37831, USA*

[4]*Idaho National Laboratory, Idaho Falls, Idaho 83415, USA*

(Received 8 May 2019; published 28 June 2019)

The impact of anharmonicity on the vibrational entropy and heat capacity of UO_2 has been investigated from 10 to 1200 K using inelastic neutron-scattering measurements of the phonon density of states (PDOS). Small changes in the PDOS are observed from 10 to 295 K, with more noticeable changes appearing in the 750- and 1200-K data. The specific heat determined from the PDOS measurements is in agreement with macroscopic specific heat measurements, and the overall impact of nondilation anharmonicity on the specific heat has been shown to be less than 2%. An analysis of the phonon measurements shows that the softening of acoustic phonons with temperature is consistent with the quasiharmonic approximation. The optical phonons deviate from the quasiharmonic prediction, with the low-energy optical phonons between approximately 20 and 50 meV softening more than expected, while the higher-energy optical phonons between approximately 50 and 80 meV have no appreciable softening over the temperature range measured. The observation of a small anharmonic specific heat contribution has been shown to be the result of relatively large energy-dependent anharmonic effects which have opposite sign, leading to a total contribution near zero.

DOI: 10.1103/PhysRevMaterials.3.065405

I. INTRODUCTION

In uranium dioxide (UO_2), the consequences of $5f$ electrons have been the subject of several experimental and theoretical studies and present a serious challenge to the modeling of material properties. Measurements of the phonon lifetimes and thermal conductivity [1], for example, are in disagreement with advanced simulations using dynamical mean-field theory (DMFT) [2]. The observed phonon linewidth broadening and thermal conductivity are a result of the anharmonicity of UO_2. However, a detailed account of how anharmonicity shapes other thermodynamic properties of UO_2 has not been explored.

The technological importance of UO_2 as a nuclear fuel has generated intense experimental and theoretical interest in the thermodynamic properties of UO_2 for decades. Knowledge of the specific heat capacity is relevant to heat storage in reactor fuel as a potential safety issue, especially in connection with the anomalous departure from the Dulong-Petit law observed above ∼1500 K, and it enters directly into simulations of thermal transport for modeling fuel performance [3]. Moreover, the underlying physical mechanisms associated with the specific heat of UO_2 below 1500 K have been of interest in helping determine the atomic (Frenkel-pair) versus electronic type of lattice defect associated with the anomalous heat capacity above 1500 K [4].

Below 1500 K, the specific heat capacity of UO_2 is known to be dominated by the lattice vibrational entropy, including the contributions related to the harmonic phonon free energy and the so-called nonharmonic contributions associated with thermal expansion (dilation) and anharmonic phonon-phonon interactions [3,5,6]. While the harmonic component has been evaluated using the 300-K phonon dispersion measurements of Dolling *et al.* [5] and the thermal expansion contribution can be calculated as a function of temperature using thermophysical property measurements of UO_2 [6], the magnitude of the nondilation anharmonic contribution to the specific heat of UO_2 is less certain. It has been estimated to be less than 2% of the total lattice specific heat based on temperature-dependent Debye-Waller factor measurements [4,7] and is in general agreement with UO_2 enthalpy measurements [6].

However, the calculated anharmonic specific heat value has not been verified experimentally, and a negligibly small anharmonic specific heat is surprising [6,8] considering the strongly anharmonic nature of phonons in UO_2 [1,9] is responsible for the low thermal conductivity below 1500 K. That is, since anharmonic phonon linewidth broadening (arising from the cubic term of the interatomic forces) is large, it might be expected that the anharmonic specific heat contribution, which is related to phonon-phonon interactions given by the cubic and quartic interatomic forces [10,11], would be large as well. Given the observation of strong anharmonic linewidth broadening, it is of interest to investigate in detail how phonon energies and heat capacity are impacted by anharmonicity as well.

Here we report inelastic neutron-scattering measurements of the phonon density of states (PDOS) for UO_2 at 10, 77, 295, 750, and 1200 K. The PDOS measurements have been analyzed to separate the harmonic and nonharmonic components of the vibrational entropy and the heat capacity of UO_2

*bryanms@ornl.gov
†manleyme@ornl.gov

as a function of temperature. The lattice heat capacities are in agreement with macroscopic specific heat measurements [12,13], but despite the strong anharmonic phonon linewidth broadening for UO_2 [1], the anharmonic heat capacity is only a few percent and negative at 1200 K, as predicted theoretically [4,7]. The apparent inconsistency of a small anharmonic contribution to the specific heat in a material with large anharmonic phonon linewidth broadening is resolved as the result of substantial energy-dependent anharmonic contributions to the specific heat, which have opposite sign and net a contribution near zero.

II. EXPERIMENT

Inelastic neutron-scattering (INS) measurements of the PDOS for UO_2 at 10, 77, 295, 750, and 1200 K were made on the wide Angular Range Chopper Spectrometer (ARCS) at the Spallation Neutron Source [14]. The experimental setup of the spectrometer was identical to our previously reported PDOS measurements for UO_2 at 295 and 1200 K [9], but with the addition of a (1.6°) radial collimator, which provides both background reduction and better angular resolution [15]. The same polycrystalline depleted UO_2 sample, encapsulated in a vanadium can, that was used previously was used here [9]. The sample was mounted in a cryostat for the low-temperature (10, 77, 295 K) measurements and a vacuum furnace for the high-temperature (750, 1200 K) measurements. Following the procedures described in Ref. [9], three incident neutron energies E_i of 30, 60, and 120 meV were used at each temperature to collect data as a function of scattering angle ϕ and time-of-flight t. Scattering introduced by the sample can, the cryostat, and the furnace were corrected for by subtracting the corresponding spectra from a duplicate, empty sample can measurement. The corrected scattered neutron intensities, $I(\phi, t)$, were converted to the scattering function $S(Q, E)$, with Q being the momentum transfer magnitude and E being the energy transfer. The method applied to concatenate the spectra collected with the three incident energies E_i to achieve a resolution of about 3% across the entire energy-transfer range has been described elsewhere [9].

The (neutron-weighted) generalized PDOS $g^{\mathrm{NW}}(E)$ was then obtained by integrating $S(Q, E)$ over Q values ranging from 3 to 7 Å^{-1}, which corresponds to about four Brillouin zones for UO_2. Below the 30.8-K Néel transition temperature, significant scattering of magnons will be present as UO_2 is in the antiferromagnetic state. This scattering is located in the low-Q region, and the intensity decreases with increasing Q as a result of the magnetic form factor [16–18]. This scattering is not present in any other higher temperature data set but does exist in the 3–7 Å^{-1} window at 10 K. To extract the phonon DOS at low temperatures, the integration range in Q was shifted upwards, with 6.5–12.5 Å^{-1} being sufficiently high in Q based on previous measurements of the magnetic form factor as a function of Q. However, this PDOS does not include measurements made with $E_i = 30$ meV, as that data includes magnetic scattering across nearly the entire dynamic window. For comparison, we have also applied this shifted window to the 77-K data set.

The magnetic scattering and magnon density of states will also impact the heat capacity at low temperatures and is present in the 10-K data. Based on previous measurements of the dispersion in the antiferromagnetic state [19–21], as well as direct inspection of the data above and below T_N, the magnetic scattering can be located and studied. Here we have used the range $E = 0$–14 meV, $Q = 0$–4.5 Å^{-1}, using only the $E_i = 30$ meV data to extract the magnon DOS from the 10-K data. For both the magnetic and phonon density of states at low temperature, a software package called MULTIPHONONwas employed to extract a DOS from the INS data [22].

The measured neutron-weighted PDOS is expressed as

$$g^{\mathrm{NW}}(E) = \frac{\sigma_U}{M_U} g_U(E) + 2\frac{\sigma_O}{M_O} g_O(E), \tag{1}$$

where $A_U = \frac{\sigma_U}{M_U}$ and $A_O = \frac{\sigma_O}{M_O}$, with $\int_0^\infty g^{\mathrm{NW}} dE = 1$. $g_U(E)$ and $g_O(E)$ are the partial phonon DOS of uranium and oxygen atoms with $g_{\mathrm{UO_2}}(E) = g_U(E) + 2g_O(E)$. M_i is the atomic mass of element i (i = U or O), and σ_i is the corresponding neutron-scattering cross section [23]. The uranium and oxygen contributions to the total PDOS are neutron weighted, with $\frac{\sigma_O}{M_O}$ approximately 7 times larger than $\frac{\sigma_U}{M_U}$. The Debye-Waller factors e^{-2W_i} have not been included here, as such thermal effects have been determined to be small (∼1%–2%) and within the uncertainties of our PDOS measurements [9,24].

In order to extract the neutron unweighted PDOS, all modes below 25 meV were attributed to uranium and all modes above 25 meV were attributed to oxygen, consistent with partial PDOS calculations [9,25,26]. That is, we assume neutron weighting can be removed by using a step function at 25 meV, which serves as a boundary energy between oxygen and uranium modes. The effect of using a step function in the neutron-weighting correction has been tested by varying the boundary energy to determine the effect on thermodynamic results. The thermodynamic results of all three cases (20, 25, and 30 meV) vary within only a few percent. Therefore a 25-meV boundary energy was used at all temperatures to remove neutron weight from the data.

The heat capacity of UO_2 single crystal was measured using a thermal relaxation method in a commercially available Quantum Design physical properties measurement system (DynaCool-9). Measurements were performed from 1.8 to 302 K.

III. RESULTS

Neutron-weighted PDOS spectra of UO_2 measured at 77, 295, 750, and 1200 K are shown in the top panel of Fig. 1. The spectra at 295 and 1200 K are essentially the same as our previously reported PDOS measurements [9] but with slightly sharper features than those reported in Ref. [9] as a result of the previously mentioned insertion of a radial collimator between the sample and the detectors on the ARCS beamline [15].

Well-defined zone-boundary phonon peaks are observed at energies of 12, 21, 33, 56, and 72 meV at 77 K. With reference to the single-crystal phonon dispersion measurements [1,9], the 12- and 21-meV peaks correspond to the uranium-dominated transverse acoustic (TA) and the longitudinal acoustic (LA) zone-boundary energies. The remaining peaks

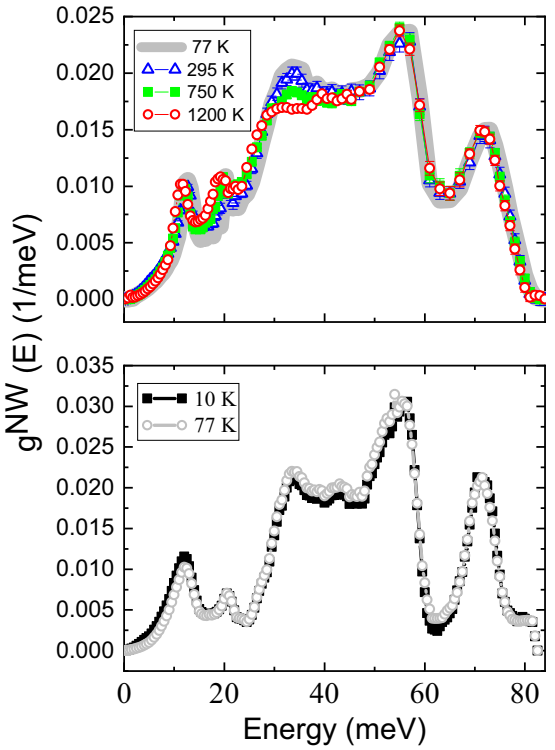

FIG. 1. Top panel: neutron-weighted phonon density of states for 77 K, shown as a gray line, 293 K, shown as blue triangles, 750 K, shown as green diamonds, and 1200 K, shown as red circles. A Q integration range of 3–7 Å^{-1} was used. Well-defined peaks occur at the zone boundaries at 12, 21, 33, 56, 72, and 76 meV. In the bottom panel, neutron-weighted phonon density of states in the antiferromagnetic state at 10 K, shown as black circles, and in the paramagnetic state at 77 K, shown as gray diamonds. The integration range for both temperatures was modified to exclude the magnetic scattering. The range used here is 6.5–12.5 Å^{-1}. The phonon density of states shows no significant changes in this temperature range.

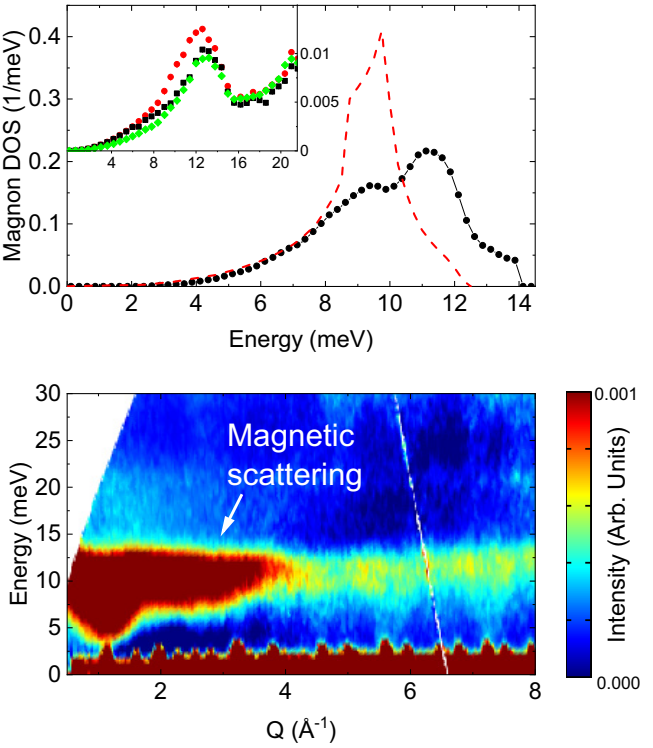

FIG. 2. Top panel, the measured density of states in the region $E = 0$–14 meV, $Q = 0$–4.5 Å^{-1} at 10 K, shown as black circles from INS. This region shows significant scattering only at 10 K, attributed to the magnon DOS. A previous magnon DOS [28], based on a model dispersion from INS data [19], is shown as a red dashed line. The inset shows the PDOS over a similar energy range, with an integration range of Q from 6 to 8 Å^{-1}, with the 10-, 77-, and 295-K data shown as red circles, black squares, and green diamonds, respectively. The bottom panel shows a color contour plot of the dynamic structure factor, $S(Q, E)$, with the magnetic scattering primarily shown as the red, intense scattering in the low-energy and low-Q region indicated by the arrow.

(33, 56, and 72 meV) correspond to the oxygen-dominated transverse-optical (TO1 and TO2) and the longitudinal-optical LO2 modes, respectively. In general, the positions of the PDOS peaks shift to lower energies with increasing temperature as a result of lattice expansion. We note that the high-energy optical TO2 and LO2 phonon peaks soften by less than 1 meV out of 55 and 72 meV, respectively, as the temperature increases from 77 to 1200 K, while the lower-energy TA, LA, and TO1 phonons soften more perceptibly from 12, 21, and 33 meV to 11, 19, and 30 meV, respectively. This is particularly true in the energy range of 20–40 meV in which the LA phonon peak at 21 meV is blurred to a broader peak and the TO1 phonons at 33 meV are diminished from a resolved peak at 77 K to a broad shoulder at 1200 K.

The resulting PDOS for 10 and 77 K are plotted in the bottom panel of Fig. 1, with a shifted integration region to avoid magnetic scattering (shown in the bottom panel of Fig. 2) in the 10-K data. No significant difference between the two temperatures is evident. Differences as a result of the integration range can be seen in the 77-K data shown in the top and bottom panels of Fig. 1 and are not the result of changes in the PDOS as a function of temperature. Zone-boundary peaks observed with this integration range are also in agreement with previous measurements of the dispersion [9].

Figure 2 shows the magnon density of states measured in the range $E = 0$–14 meV, $Q = 0$–4.5 Å^{-1}, in the top panel. In the bottom panel of Fig. 2, the dynamic structure factor $S(Q, E)$ is shown with the magnetic scattering primarily shown in red. With increasing Q, the magnetic scattering decreases, and at high Q (above 6.5 Å^{-1}), only phonon scattering remains, and the resulting PDOS is nearly identical to the PDOS obtained at 77 K. The measured magnon DOS here is in reasonable agreement with previous measurements of the dispersion [19–21,27] and calculated DOS based on a model dispersion [28]. Notably, no scattering is observed below 2 meV or above 14 meV, with increasingly more excitations at larger energies until a maximum, which then decreases rapidly towards zero. However, we cannot exclude other quasiparticle excitations, such as quadrupolar excitations observed previously [20,21,27] from this data set.

Within the rather large integration range of 6.5–12.5 Å^{-1}, the PDOS is in agreement between 10- and 77-K data sets, as

shown in the lower panel of Fig. 1. However, using a relatively narrow range above the magnetic scattering to calculate the PDOS (6–8 $Å^{-1}$), the 10-K PDOS is slightly larger than the 77- and 295-K PDOS between 6 and 13 meV, as shown in the inset in Fig. 2. A plausible explanation for this additional scattering is that the quadrupolar modes, as observed in the literature, occur in this energy range and this is a result of electron-phonon coupling. We find agreement across temperatures above T_N, shown in the 77- and 295-K data, when there should no longer be strong electron-phonon coupling. This additional scattering is contrary to the quasiharmonic approximation, which would predict a softening of the TA mode as temperature increases.

IV. ANALYSIS

A. Anharmonic PDOS contribution

Within the quasiharmonic (QH) approximation, thermal-expansion-induced phonon softening shifts the phonon energies proportionally downward throughout the PDOS spectrum. The softened PDOS as a function of temperature T, $g_T^{\mathrm{QH}}(E')$, relative to a reference temperature T_0 can be written as

$$g_T^{\mathrm{QH}}(E') = g_{T_0}[E(1-3\alpha\gamma)], \tag{2}$$

where $\Delta V/V = 3\alpha$, and γ is the average (macroscopic) Grüneisen parameter given by $\frac{3\alpha BV}{C_V}$, with C_V, B, V and α being the harmonic specific heat, bulk modulus, molar volume, and linear thermal expansion coefficient, respectively. These parameters are temperature dependent and are reported in the literature [29,30]. This generates a PDOS at some temperature T from the PDOS at a reference temperature T_0, with a rescaled energy determined by $(1-3\alpha\gamma)$.

We have used Eq. (2) to calculate the quasiharmonic (i.e., energy-shifted) spectrum g_T^{QH} for $T = 295$, 750, and 1200 K using the PDOS spectrum at 77 K as a reference T_0. The reference temperature of 77 K was used for the QH calculations to ensure that the measured phonon spectrum used as a reference is not affected significantly by magnons in the antiferromagnetic state of UO_2 (see bottom panel, Fig. 2). Given the very small changes in PDOS and QH approximation parameters between 10 and 77 K, this results in virtually no change in the QH prediction. In addition to calculating the energy shift (softening) due to thermal expansion using Eq. (2), we have introduced anharmonic phonon linewidth broadening into the QH-PDOS spectra by convolution with phonon linewidths measured on UO_2 single crystals at 295 and 1200 K, as described previously [9]. These linewidth convoluted quasiharmonic spectra, $g_T^{\mathrm{QH}\otimes\mathrm{Width}}$, are plotted as the solid red lines in Fig. 3 along with the corresponding PDOS measurements g^{NW} (symbols) at 295, 750, and 1200 K. The phonon linewidth distribution for 750 K was determined by interpolation of the linewidth results for 295 and 1200 K.

The difference between the quasiharmonic spectrum $g_T^{\mathrm{QH}\otimes\mathrm{Width}}$ and the measured PDOS spectrum,

$$g_T^{\mathrm{Anh}} = g_T^{\mathrm{NW}} - g_T^{\mathrm{QH}\otimes\mathrm{Width}}, \tag{3}$$

represents the anharmonic contribution g^{Anh} to the PDOS beyond the nonharmonic dilation of the lattice accounted for in the quasiharmonic expansion. These variations, g_T^{Anh}, are shown as the thick blue lines in Fig. 3 and represent a determination of the anharmonic contributions to the PDOS of UO_2 at 295, 750, and 1200 K.

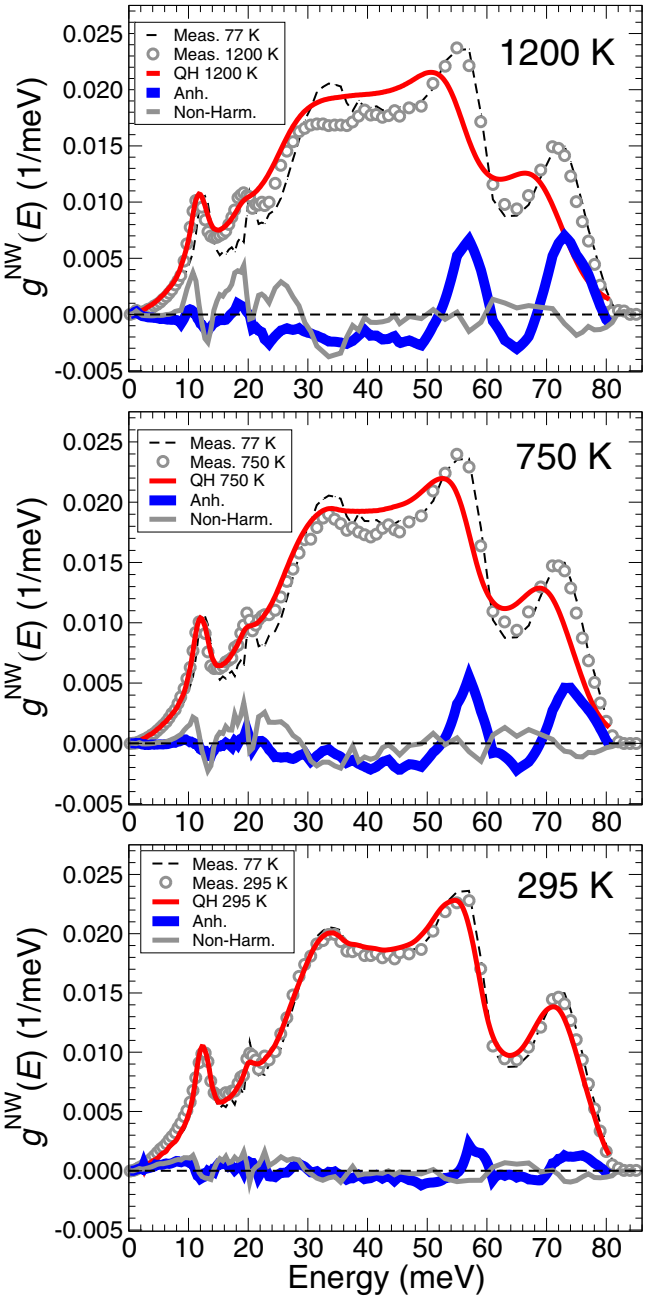

FIG. 3. Neutron-weighted phonon density of states, plotted at 295 K (bottom), 750 K (middle), and 1200 K (top) as open circles. For reference, the T_0 data taken at 77 K is plotted as a dashed line in each panel. The quasiharmonic approximation at each temperature, convoluted with measured phonon linewidths, is plotted as a red line. The difference between the neutron-weighted PDOS and the quasiharmonic approximation, the anharmonic contribution, is shown as a blue line for each temperature. The nonharmonic change in the measured PDOS, the difference between the measured PDOS at high temperature, and the measured PDOS at 77 K are shown as a gray line.

At 295 K, the anharmonic contribution is relatively insignificant with only small positive contributions near 56 and 72 meV, which correspond to the optical TO2 and LO2 phonon peaks. This result illustrates that the experimentally measured PDOS spectrum of UO_2 at 295 K can be explained quite well from the 77-K measurements using quasiharmonic thermal expansion and corrections for linewidth broadening. For higher temperatures, however, the $g_T^{\mathrm{QH}\otimes\mathrm{Width}}$ spectra deviate increasingly from the measured PDOS. The anharmonic impact on the PDOS spectra can be divided into three phonon energy intervals: approximately 0–20 meV corresponding to the uranium-dominated acoustic phonons; approximately 20–50 meV corresponding to the oxygen-dominated optical TO1 and LO1 phonons; and approximately 50–80 meV corresponding to the oxygen-dominated high-energy TO2 and LO2 phonons.

For energies below 20 meV the observed acoustic phonon energy shifts are in general agreement with quasiharmonic approximation, and g_T^{Anh} is negligible in this energy range up to the highest measured temperature, 1200 K. However, between ~20 and 50 meV, there is a continuous negative anharmonic contribution at 750 K that nearly doubles in magnitude at 1200 K. This negative g_T^{Anh} contribution exists because the TO1 and the LO1 phonons in this range soften in energy more than the ~3% predicted by the QH approximation. This effect is even larger at 1200 K, where the measured phonon energy softening for the TO1 and the LO1 phonons becomes ~10% (i.e., softens from 33 to 30 meV) compared to the 6% shift predicted by the QH approximation. At high temperatures, the TO2 and LO2 phonons have a large contribution to g_T^{Anh} at 56 and 72 meV. This is attributed to the stiffness of the TO2 and LO2 optical phonons relative to the QH approximation. The acoustic phonon energies tend to follow the QH approximation, softening from 77 to 1200 K. The TO1 and LO1 optical phonons soften much more than predicted by the QH approximation, and the TO2 and LO2 optical phonons soften much less than predicted by the QH approximation.

The neutron weighted PDOS presented in Figs. 1 and 3 lead to two temperature regimes. In the low-temperature regime, the 10-K, 77-K, and 295-K PDOS show little change as a function of temperature and generally follow the QH prediction. In the high-temperature regime, the 750-K and 1200-K data show deviations from the QH prediction. Therefore our analysis of the thermodynamic properties from the PDOS will be split into low-temperature results ($T \leqslant 295$ K) and high-temperature results ($295 < T < 1200$ K).

B. Vibrational entropy

The total vibrational entropy S_{ph} per unit cell at temperature T can be written as

$$S_{\mathrm{ph}}(T) = 3Nk_B \int_0^\infty g_T[(n_T+1)\ln(n_T+1) - n_T \ln(n_T)]dE, \tag{4}$$

where $n_T = 1/(e^{E/k_BT} - 1)$ is the Planck distribution function, and $N = 3$ for UO_2 with three atoms in the unit cell, k_B is Boltzmann's constant, and g_T is the neutron-unweighted PDOS at temperature T. Separating the vibrational entropy into harmonic (S_V) and nonharmonic (S_{NH}) terms, the harmonic entropy is a function of the harmonic phonon energy spectrum given by

$$S_V(T) = 3Nk_B \int_0^\infty g_{T_0}[(n_T+1)\ln(n_T+1) - n_T \ln(n_T)]dE, \tag{5}$$

where g_{T_0} is the unweighted harmonic PDOS at the reference temperature T_0. To a good approximation, the neutron weighting of the measured PDOS g^{NW} [see Eq. (1)] can be removed by attributing all phonons below 25 meV to the heavier uranium atoms and attributing all phonons above 25 meV to the lighter oxygen atoms. Theoretical partial PDOS are consistent with this approach [9,25,26].

Defining the nonharmonic entropy S_{NH} formally as the total phonon entropy minus the harmonic entropy,

$$S_{\mathrm{NH}}(T) = S_{\mathrm{ph}}(T) - S_V(T). \tag{6}$$

In this expression, S_{NH} is defined to contain a component S_D due to lattice expansion/dilation and an anharmonic phonon-phonon interaction component S_A. S_D is given by

$$S_D(T) = \int_{T_0}^{T} 9\alpha^2 BV\,dT, \tag{7}$$

where B, V, and α are the bulk modulus, the molar volume, and the linear thermal expansion coefficient, respectively, each of which are temperature dependent [29], and the anharmonic phonon-phonon interaction component is defined by

$$S_A(T) = S_{\mathrm{NH}}(T) - S_D(T) = S_{\mathrm{ph}}(T) - S_V(T) - S_D(T). \tag{8}$$

The temperature dependence of the nonharmonic S_{NH} and the dilation S_D entropies are plotted in Fig. 4. A linear relationship between S_{NH} and temperature is observed, as

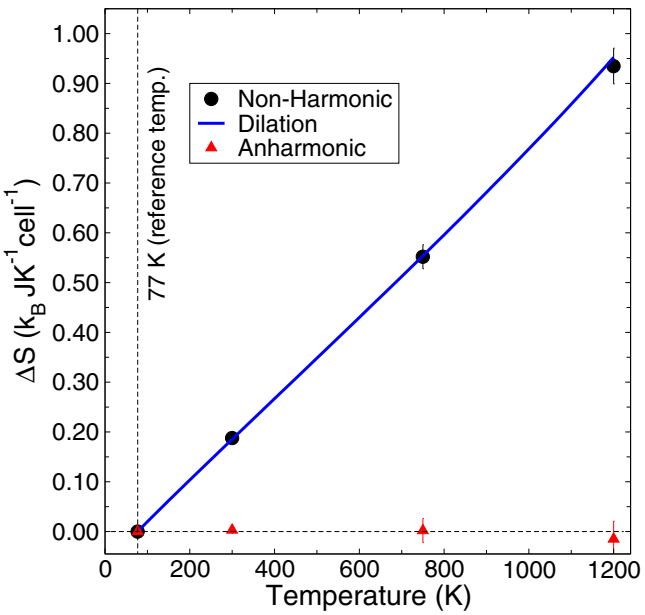

FIG. 4. The change in the nonharmonic (black points) and anharmonic (red triangles) entropy as a function of temperature. The lattice expansion/dilation entropy is shown as a blue line. The reference temperature, $T_0 = 77$ K, is marked by a vertical dotted line.

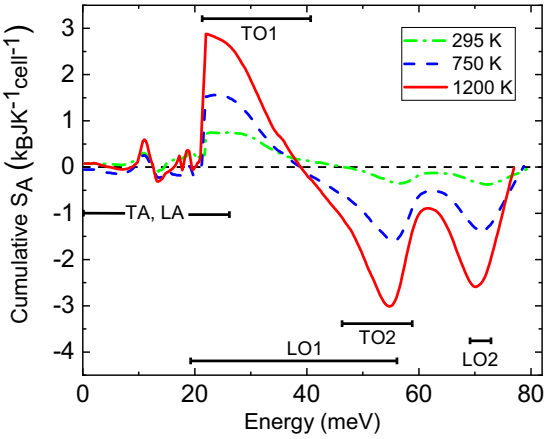

FIG. 5. The cumulative contribution from the PDOS to the anharmonic entropy, from 0 to some energy E, as a function of E. The total contribution from the PDOS is the final point near 80 meV. The 77-K PDOS was used as g_{T_0}, the reference temperature PDOS, with 295 K, 750 K, and 1200 K shown as a green dash-dot line, a blue dashed line, and red solid line, respectively. Across all three temperatures, the positive contribution of the TO1 and LO1 phonons and the negative contribution from the TO2 and LO2 phonons sum to nearly zero. Phonon modes and corresponding energy span are taken from previous measurements of the dispersion [1].

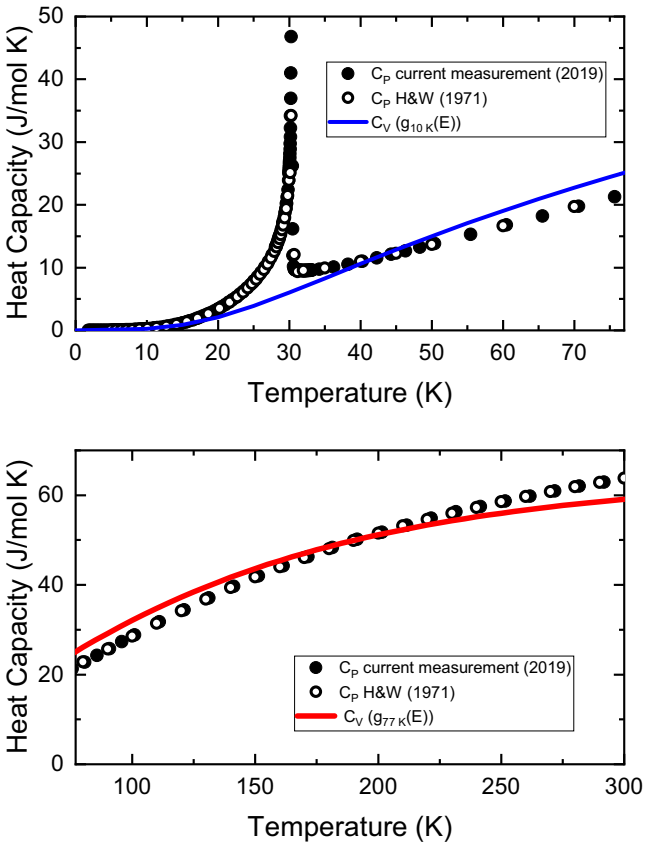

FIG. 6. Heat capacity as a function of temperature. Both panels show the previous heat capacity measurements [13] as open circles, with our own measurements as black circles. A sharp spike at the transition temperature $T_N = 30.8$ K is a result of the Néel transition from an antiferromagnetic state to a paramagnetic state. In the top panel, C_V is calculated using the 10-K PDOS as g_{T_0}. In the bottom panel, C_V is calculated using the 77-K PDOS.

expected considering the linear thermal expansion in this temperature range [6]. Overall, the expansion/dilation entropy S_D and the nonharmonic entropy S_{NH} are nearly equal because of the very small value of the anharmonic component S_A.

The anharmonic entropy is negligible despite its large impact on the phonon energy distribution as shown in Fig. 4. This can be explained by looking into the distribution of the anharmonic entropy as a function of energy. Figure 5 shows the cumulative anharmonic entropy S_A, from 0 to some phonon energy E, for 295, 750, and 1200 K. For all three temperatures, phonons below 21 meV make virtually no contribution; followed by a large initial increase, then a net negative contribution from the optical phonons between 21 and 54 meV; with an overall positive contribution from the high-energy optical phonons above 55 meV. Small differences in the measured PDOS are magnified when the data is unweighted below 25 meV. The total contribution is nearly zero at each temperature, leading to small total anharmonic entropy, as indicated by the final point of each cumulative curve.

C. Specific heat

We have further determined the lattice specific heat C_{Latt} of UO_2. We first calculated harmonic and dilation specific heat C_V and C_D using

$$C_V(T) = 3Nk_B \int_0^\infty g_{T_0} \frac{E^2}{(k_BT)^2} \frac{e^{(E/k_BT)}}{(e^{E/k_BT}-1)^2} dE, \quad (9)$$

$$C_D(T) = 9\alpha^2 BVT. \quad (10)$$

The nonharmonic specific heat C_{NH} is

$$C_{\mathrm{NH}}(T) = T\frac{\partial S_{\mathrm{NH}}}{\partial T}, \quad (11)$$

from which we can calculate the total anharmonic specific heat by taking into account the specific heat of dilation,

$$C_A(T) = C_{\mathrm{NH}}(T) - C_D(T). \quad (12)$$

Summation of the harmonic, dilation, and anharmonic specific heat yields the lattice specific heat C_{Latt},

$$C_{\mathrm{Latt}}(T) = C_V(T) + C_D(T) + C_A(T). \quad (13)$$

Past measurements of the heat capacity [13] in the low-temperature regime ($T < 295$ K) are in good agreement with our own heat capacity measurements, shown with the calculated heat capacity in Fig. 6. While our current measurements use a single-crystal sample, the past measurements used sintered powder. In this low-temperature regime, there are only small changes in the PDOS and as a result, only very small nonharmonic contributions to the heat capacity (<2 J/mol K). The resulting heat capacity C_{Latt} is close to the harmonic heat capacity C_V. Relatively good agreement is found between the calculated and measured heat capacity,

except in the vicinity of T_N, where magnetic contributions are large. The magnetic contribution to the heat capacity, C_M, has been previously found to be large at temperatures below T_N [28,31,32], much larger than the contribution from the lattice. However, the calculated low temperature C_V is very sensitive to the low-energy modes in the PDOS, which are not accurately determined in our measurements. Therefore we cannot make a detailed comparison between the measured heat capacity and the sum of C_{Latt} and C_M, which was done previously [28,31,32]. The crystal field specific heat, C_{CF}, can be calculated from Refs. [33–35], but they are on the order of 1 J/mol K at largest in the low-temperature regime and have not been included in the low-temperature regime. Away from the transition, the agreement between C_V, C_{Latt}, and the measured C_P have values of 59.7, 59.1, and 63.8 J/mol K, respectively, at 295 K. This moderate agreement (within 5%) is a result of the small anharmonic effects which are evident by the PDOS showing little change in this temperature range, a small value of C_D, and no contribution from the magnetic behavior far above from T_N.

The calculated C_V using the 295-K PDOS is shown in Fig. 7, in the high-temperature regime ($T > 295$ K). C_V has a value of 64.9 J/mol K at 400 K. This is different than the measured value of C_P, 71.3 J/mol K. At this temperature and above, the harmonic heat capacity is still the dominant contribution to the total heat capacity, but the electronic, dilation, and anharmonic effects begin to be significant. As a result, the harmonic curve and the measured C_P begin to show significant separation in Fig. 7. As C_V increases with temperature, it approaches the Dulong-Petit value of $3\mathrm{Nk}_B$ in the high-temperature limit, significantly lower than the measured C_P values. The quasiharmonic ($C_V + C_D$) and the total lattice specific heat C_{Latt} ($C_V + C_D + C_A$) are also plotted in Fig. 7. C_{Latt} is found to be very close to the quasiharmonic heat capacity, with the anharmonic specific heat close to zero below 400 K and slightly positive ($\leqslant 1$ J/mol K) up to 1000 K, and then slightly negative, approaching approximately -1 ± 1 J/mol K at 1200 K. The thermodynamic relation $C_D = C_P - C_V$ is clearly not true at high temperatures, as the quasiharmonic curve $C_V + C_D$ is significantly different than measured C_P values. Therefore additional contributions to the specific heat, such as the known crystal field contribution [33–35], must be taken into account. By adding the crystal field specific heat, C_{CF}, to the harmonic term C_V there is still a significant discrepancy between the measured and calculated values. With the total lattice contribution C_{Latt} and C_{CF}, the total specific heat is in excellent agreement with the macroscopic specific heat measurements for UO_2 by calorimetry [12,13] in this temperature regime.

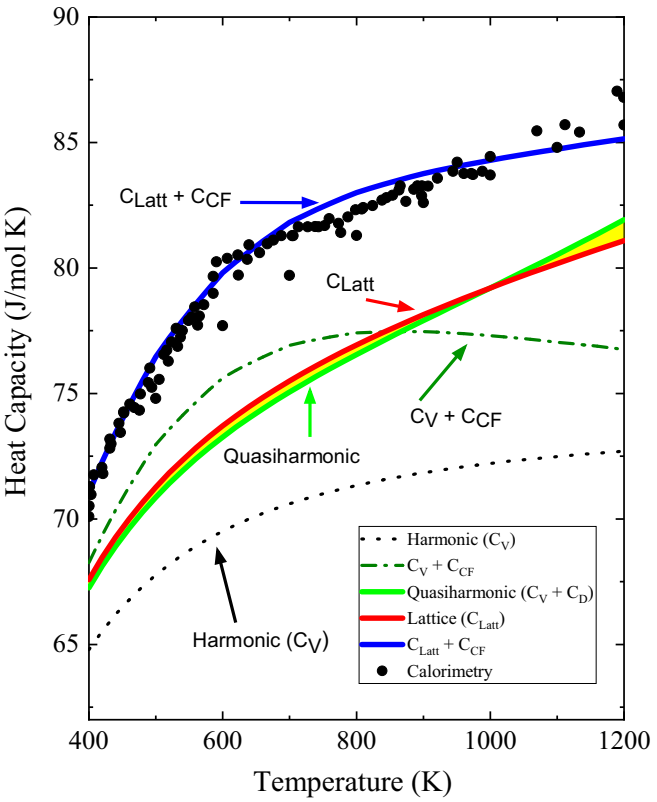

FIG. 7. Heat capacity as a function of temperature. Calorimetry measurements are shown as black points, from [12,13,36,37]. The harmonic heat capacity, C_V, is shown as a black dotted line. The electronic and harmonic heat capacity, $C_V + C_{\mathrm{CF}}$, is shown as a green dash-dot line. The total lattice heat capacity, C_{Latt}, is shown as a red line. The quasiharmonic heat capacity, $C_V + C_D$, is shown as a green line, with the difference between quasiharmonic and lattice heat capacity, the anharmonic corrections, shaded in yellow. The lattice specific heat from the PDOS is added to the crystal field specific heat to produce the blue curve, $C_{\mathrm{Latt}} + C_{\mathrm{CF}}$, in agreement with calorimetry measurements of C_P.

V. DISCUSSION

Our measurements show the impact of anharmonicity on the phonon energies and heat capacity in UO_2. The overall small anharmonic entropy and anharmonic specific heat are the result of both large positive and negative contributions from different optical phonon energy ranges, which lead to a total contribution near zero. The quasiharmonic heat capacity is based on noninteracting phonons and thermal expansion of the lattice, shown as a green line in Fig. 7, and does not take additional nonharmonic effects into account. If the total anharmonic contribution to the heat capacity were large, the lattice heat capacity would reflect it, but not the quasiharmonic. However, we find agreement between the quasiharmonic and lattice heat capacity in UO_2. That is, despite the noticeable disagreements between the quasiharmonic PDOS and the measured PDOS at higher temperatures shown in Fig. 3, the low total anharmonic contribution leads to relatively close agreement between the quasiharmonic and lattice heat capacity.

Anharmonicity has been measured in the phonons of this system with phonon dispersion and linewidth measurements [1], and significantly impacts the thermal conductivity. It was also observed that the LO1 mode contributes the most to the thermal conductivity at 295 K and also contributes significantly at 1200 K. It is interesting to note that the LO1 and TO1 phonon modes are located between 30 and 50 meV, and the corresponding region in the PDOS, shown in Fig. 3, deviates from both the quasiharmonic and low-temperature measurements. Outside of this region, the acoustic phonons

generally agree with the quasiharmonic prediction, and the TO2 and LO2 modes agree with the low-temperature PDOS. The LO1 and TO1 regions contribute negatively to the entropy, shown in Fig. 5, which is offset by the positive contributions below 30 meV and above 50 meV. While the anharmonicity and phonon lifetimes determine the thermal conductivity, the overall effect of anharmonicity on the heat capacity in this system is relatively small as a result of the offsetting contributions to the anharmonic entropy of the different phonon regions.

Examination of the energy shifts in the PDOS indicates the low-energy TO1 and LO1 phonons (below 50 meV) respond to temperature very differently from the high-energy TO2 and LO2 optical phonons. The large softening of the low-energy optical phonons combined with the negligible energy shifts of the high-energy optical phonons widens the energy range of the optical phonons as temperature increases. It is clear that this behavior of the optical phonons is in contrast with the quasiharmonic assumption that all phonons should soften in energy. This explains the relatively poor agreement between our previously measured PDOS for UO_2 with the first-principles simulations based on the quasiharmonic approximations [9]. The anisotropy introduced by the quadrupoles in UO_2 may also introduce distortion of the optical phonons through spin-lattice coupling [38–40]. The results suggest that more advanced approaches based on dynamical mean-field theory or quantum Monte Carlo could include the finite-temperature effects intrinsically, and combined with an appropriate account of the spin-lattice coupling of UO_2, are likely to be essential to predict the anharmonic phonon behavior.

Measurements of the PDOS as a function of temperature here lead to splitting the heat capacity into a low-temperature ($T \leqslant 295$ K) and a high-temperature ($295 < T < 1200$ K) regime. That is, there is relatively little change in the PDOS from 10 to 295 K but substantial changes between the 295-, 750-, and 1200-K results. Considering these two separate regimes allows one to model the measured heat capacity C_P in two different ways. X-ray and neutron diffraction measurements from 300 to 1673 K also suggest a regime from 300 to 1200 K, along with another regime from 1200 to 1673 K [41,42] based on the coefficient of thermal expansion and lattice parameter measurements. Above 1200 K, the lattice parameter increases with temperature beyond the usual thermal expansion behavior observed below 1200 K, and the various contributions to C_P are likely different. For example, C_P can be accounted for by considering the contributions from harmonic phonons, thermal expansion, and polarons alone above 1200 K. A PDOS measured in this temperature range may therefore differ substantially from our measurement at 1200 K. However, within our temperature range from 10 to 1200 K, we see no evidence of a polaron or anti-Frenkel defect contribution, consistent with the previous results [3,41,43,44].

VI. CONCLUSIONS

Time-of-flight INS measurements of the phonon density of states, from 10 to 1200 K, are reported in this paper. Between 10 and 295 K, there is little change in the PDOS with temperature, and the harmonic heat capacity calculated from the PDOS accounts for the measured heat capacity. Measurements of the heat capacity from 2 to 300 K are in agreement with previous results for UO_2. Above 400 K, the lattice, dilation, and crystal field contributions to the heat capacity are significant. Only when all of these contributions are taken into account can the calculated heat capacity match previous experimental measurements. Low-energy optical modes below 50 meV respond very differently than high-energy optical modes above 50 meV. The former soften with temperature, and the latter do not change significantly up to 1200 K. As a result, the phonon spectrum deviates from the quasiharmonic approximation. The anharmonic effects from the optical modes are large but with opposite sign, leading to a total anharmonic entropy near zero. More advanced simulation techniques, such as dynamic mean-field theory or quantum Monte Carlo, may be necessary to capture the temperature-dependent behavior of the optic modes.

ACKNOWLEDGMENTS

We would like to thank K. J. McClellan, A. D. Andersson, and C. R. Stanek of Los Alamos National Laboratory for providing the UO_2 powder (INS) and single-crystal (heat-capacity) samples. M.S.B., M.E.M., and K.G. were supported by the Center for Thermal Energy Transport under Irradiation, an Energy Frontier Research Center funded by the U.S. Department of Energy (DOE), Office of Science, United States Office of Basic Energy Sciences. J.W.L.P., A.C., and B.C.L. were supported by the Center for Materials Science of Nuclear Fuel, an Energy Frontier Research Center funded by the U.S. Department of Energy. Portions of this research used resources at the Spallation Neutron Source, a U.S. DOE Office of Science User Facility operated by Oak Ridge National Laboratory.

[1] J. W. L. Pang, W. J. L. Buyers, A. Chernatynskiy, M. D. Lumsden, B. C. Larson, and S. R. Phillpot, Phys. Rev. Lett. **110**, 157401 (2013).
[2] Q. Yin and S. Y. Savrasov, Phys. Rev. Lett. **100**, 225504 (2008).
[3] P. Browning, J. Nucl. Mater. **98**, 345 (1981).
[4] G. Hyland and A. Stoneham, J. Nucl. Mater. **96**, 1 (1981).
[5] G. Dolling, R. Cowley, and A. Woods, Can. J. Phys. **43**, 1397 (1965).
[6] J. Fink, Int. J. Thermophys. **3**, 165 (1982).
[7] B. Willis and R. Hazell, Acta Crystallogr., Sect. A: Cryst. Phys., Diffr., Theor. Gen. Crystallogr. **36**, 582 (1980).
[8] B. Dawson, A. T. Hurley, and V. Maslen, Proc. R. Soc. London A **298**, 289 (1967).

[9] J. W. L. Pang, A. Chernatynskiy, B. C. Larson, W. J. L. Buyers, D. L. Abernathy, K. J. McClellan, and S. R. Phillpot, Phys. Rev. B **89**, 115132 (2014).
[10] R. Cowley, Adv. Phys. **12**, 421 (1963).
[11] A. Maradudin, P. Flinn, and R. Coldwell-Horsfall, Ann. Phys. **15**, 360 (1961).
[12] F. Grønvold, N. J. Kveseth, A. Sveen, and J. Tichý, J. Chem. Thermodyn. **2**, 665 (1970).
[13] J. J. Huntzicker and E. F. Westrum, J. Chem. Thermodyn. **3**, 61 (1971).
[14] D. L. Abernathy, M. B. Stone, M. Loguillo, M. Lucas, O. Delaire, X. Tang, J. Lin, and B. Fultz, Rev. Sci. Instrum. **83**, 015114 (2012).
[15] M. B. Stone, J. L. Niedziela, M. Loguillo, M. A. Overbay, and D. L. Abernathy, Rev. Sci. Instrum. **85**, 085101 (2014).
[16] A. J. Freeman, J. P. Desclaux, G. H. Lander, and J. Faber, Phys. Rev. B **13**, 1168 (1976).
[17] F. Wedgwood, J. Phys. C **5**, 2427 (1972).
[18] J. Faber and G. H. Lander, Phys. Rev. B **14**, 1151 (1976).
[19] R. A. Cowley and G. Dolling, Phys. Rev. **167**, 464 (1968).
[20] R. Caciuffo, P. Santini, S. Carretta, G. Amoretti, A. Hiess, N. Magnani, L.-P. Regnault, and G. H. Lander, Phys. Rev. B **84**, 104409 (2011).
[21] R. Caciuffo, G. Amoretti, P. Santini, G. H. Lander, J. Kulda, and P. de V. Du Plessis, Phys. Rev. B **59**, 13892 (1999).
[22] J. Y. Lin, F. Islam, and M. Kresh, J. Open Source Software **3** 440 (2018).
[23] V. F. Sears, Neutron News **3**, 26 (1992).
[24] B. Willis, Proc. R. Soc. London, Ser. A **274**, 134 (1963).
[25] T. Arima, S. Yamasaki, Y. Inagaki, and K. Idemitsu, J. Alloys Compd. **400**, 43 (2005).
[26] P. Goel, N. Choudhury, and S. Chaplot, J. Phys.: Condens. Matter **19**, 386239 (2007).
[27] S. Carretta, P. Santini, R. Caciuffo, and G. Amoretti, Phys. Rev. Lett. **105**, 167201 (2010).
[28] A. Cracknell and S. Joshua, Phys. Status Solidi B **36**, 737 (1969).
[29] J. Fink, J. Nucl. Mater. **279**, 1 (2000).
[30] D. Martin, High Temp.-High Press. **21**, 13 (1989).
[31] G. Khattak, Phys. Status Solidi A **75**, 317 (1983).
[32] R. De Batist, R. Gevers, and M. Verschueren, Phys. Status Solidi B **19**, 77 (1967).
[33] G. Amoretti, A. Blaise, R. Caciuffo, J. M. Fournier, M. T. Hutchings, R. Osborn, and A. D. Taylor, Phys. Rev. B **40**, 1856 (1989).
[34] J. G. Tobin, S.-W. Yu, C. H. Booth, T. Tyliszczak, D. K. Shuh, G. van der Laan, D. Sokaras, D. Nordlund, T.-C. Weng, and P. S. Bagus, Phys. Rev. B **92**, 035111 (2015).
[35] S. Kern, C.-K. Loong, and G. H. Lander, Phys. Rev. B **32**, 3051 (1985).
[36] H. Inaba, K. Naito, and M. Oguma, J. Nucl. Mater. **149**, 341 (1987).
[37] M. Amaya, K. Une, and M. Hirai, J. Nucl. Sci. Technol. **41**, 108 (2004).
[38] M. Wilson, P. A. Madden, and B. J. Costa-Cabral, J. Phys. Chem. **100**, 1227 (1996).
[39] S.-T. Pi, R. Nanguneri, and S. Savrasov, Phys. Rev. B **90**, 045148 (2014).
[40] S.-T. Pi, R. Nanguneri, and S. Savrasov, Phys. Rev. Lett. **112**, 077203 (2014).
[41] P. Ruello, L. Desgranges, G. Baldinozzi, G. Calvarin, T. Hansen, G. Petot-Ervas, and C. Petot, J. Phys. Chem. Solids **66**, 823 (2005).
[42] M. T. Hutchings, J. Chem. Soc., Faraday Trans. 2 **83**, 1083 (1987).
[43] G. Hyland and J. Ralph, High Temp. High Press. **15**, 179 (1983).
[44] C. Ronchi and G. Hyland, J. Alloys Compd. **213–214**, 159 (1994).